Interplay of Charge Density and Relative Humidity on the Structure of Nitrate Layered Double Hydroxides

Matías Jobbágy*,†,‡ and Nobuo Iyi§

CONICET-INQUIMAE, Facultad de Ciencias Exactas y Naturales, Universidad de Buenos Aires, Pabellón II, Ciudad Universitaria, C1428EHA-Buenos Aires, Argentina, Centro Interdisciplinario de Nanociencia y Nanotecnología, Argentina, National Institute for Materials Science (NIMS), Namiki 1-1, Tsukuba, Ibaraki 305-0044, Japan

Received: August 19, 2010; Revised Manuscript Received: September 23, 2010

The structure of several crystalline Ni(II)−Al(III) and Mg(II)−Al(III) layered double hydroxides (LDHs) intercalated with nitrate anions was studied as a function of the relative humidity. For low charge density LDHs, the electrostatic attraction between the anions and the positive LDH layers prevails over any other interaction, and the anions remain flat, *F*, with their C_3 axis perpendicular to the *xy* planes, irrespective of water activity. For LDHs bearing higher charge densities, the incoming water molecules drive an abrupt phase expansion in which the anions tilt their C_3 axis with respect to the interlamellar *xy* plane, thus resulting in an expanded, *T*, form. The structural *F*−*T* transition is discontinuous, and involves a second staging phase intermediate, with alternated *F* and *T* galleries. For intermediate charge density LDHs, the hydration process easily reverts, once the samples are resubmitted to a dry atmosphere. Dehydration of high charge density LDHs is however kinetically hindered; this behavior is explained in terms of the structural features of the involved phases. For all samples, the maximum net gallery expansion is proportional to the layer charge density, irrespective of the nature of the divalent cation.

Introduction

Layered double hydroxides (LDHs), also known as anionic clays, exhibit relevant and diverse applications, such as anion adsorptive and/or exchanging phases, electroactive solids, heterogeneous catalysts, or hybrid intercalation compounds, among others.[1] These crystalline compounds are derived from the mineral hydrotalcite (hereafter HT), $Mg_{1-x}Al_x(OH)_2(CO_3)_{x/2}\cdot nH_2O$, a natural occurring LDH phase, which consists in divalent metal cations located in the center of OH octahedra. These octahedra are connected to each other by edge-sharing OHs to form a 2D infinite sheet as they do in the basic structure of brucite $Mg(OH)_2$.[2] Isomorphic substitution of divalent cations by trivalent ones produces a permanent and very homogeneous positive charge that is homogeneously distributed along the sheets.[3,4] The charge of the layers is governed by the ratio Mg(II) to Al(III), which ranges between 2 and 4. To compensate the positive charge, anions are intercalated within the space contained between brucitelike layers (also referred as gallery or interlamellar space). The remaining interlamellar volume is filled by water molecules.

Because of the relevance of synthetic LDHs, different structural features were studied as a function of thermal treatment,[5,6] anion exchange,[7,8] or composition.[9,10] Focused on the latter issue, Xu et al. performed a thorough structural study on a family of $Mg_{1-x}Al_x(OH)_2(NO_3)_x\cdot nH_2O$ of varying *x*, and reported an abrupt change in the interlamellar distance when the Al(III) mole ratio increased from 0.2 to 0.33.[9] They reached the conclusion that the increase of the layer charge density induces a modification of the arrengement of NO_3^- anions, from a flat configuration (parallel to the brucitic layers) to a tilted one, in which the interlamellar distance expands. This observation was later supported by molecular dynamics calculations.[11] Despite these conclusions are in line with recent experimental evidence gathered by polarized ATR-FTIR spectroscopy,[12] most experimental studies report ambiguous structural results, for nitrate containing LDHs bearing *x* values nearby 0.25; most of the reported patterns are characterized by broad and even asymmetric interlamellar reflections.[8,13−17] Very recently, Iyi et al. demonstrate that the configuration of NO_3^- anions in HT also depends strongly on the water activity, a variable that it is not always controlled.[10] The aim of the present study is to assess the combined influence of layer charge density and water activity on the orientation of intercalated nitrate ions. Previous results are discussed under the light of the present findings;[18,19] kinetic aspects related to the studied process are also discussed.

Experimental Section

Highly crystalline carbonate LDHs were used as starting materials. Either synthetic ($Mg_{0.66}Al_{0.34}(OH)_2(CO_3)_{0.17}\cdot nH_2O$) or commercial ($Mg_{0.74}Al_{0.26}(OH)_2(CO_3)_{0.13}\cdot nH_2O$, Kyowa Kagaku, DHT-6) hydrotalcites were prepared following the procedures described Iyi et al.[20−22] Synthetic takovites (hereafter TK), $Ni_{1-x}Al_x(OH)_2(CO_3)_{x/2}\cdot nH_2O$, were prepared by hydrothermal decomposition of urea, according to procedures published elsewhere.[23] These carbonate LDH phases were acid-exchanged with chloride, and afterward with nitrate anions.[24,25] Elemental analysis of the samples before and after anion exchange were carried out in a Carlo Erba CHON-S analyzer. Contents of Ni, Mg, and Al were determined by inductively coupled plasma (ICP) atomic emission spectroscopy. Powder X-ray diffraction (PXRD) was conducted at a scanning speed of 2 degrees/min using a Rigaku RINT 1200 diffractometer with Ni-filtered CuK_α radiation ($\lambda = 0.15418$ nm). The relative humidity (RH) of the inlet N_2 flow was monitored with a Vaisala RH sensor (HMI41,

* To whom correspondence should be addressed. E-mail: jobbag@qi.fcen.uba.ar.
† Universidad de Buenos Aires.
‡ Centro Interdisciplinario de Nanociencia y Nanotecnología.
§ National Institute for Materials Science (NIMS).

10.1021/jp1078778
Published on Web 10/05/2010

TABLE 1: Composition and Charge Density of LDH Samples

sample	chemical composition (expressed on dry basis)	charge density 10^2 (q_e/Å^2)
HT2	$Mg_{0.66}Al_{0.34}(OH)_2(NO_3)_{0.34}$	4.29(1)
HT3	$Mg_{0.74}Al_{0.26}(OH)_2(NO_3)_{0.26}$	3.22(1)
TK2	$Ni_{0.68}Al_{0.32}(OH)_2(NO_3)_{0.33}$	4.02(1)
TK2.5	$Ni_{0.71}Al_{0.29}(OH)_2(NO_3)_{0.29}$	3.63(1)
TK3	$Ni_{0.76}Al_{0.24}(OH)_2(NO_3)_{0.24}$	3.05(1)
TK4	$Ni_{0.8}Al_{0.2}(OH)_2(NO_3)_{0.20}$	2.48(1)

Finland). A special PXRD sample holder was feed with a RH-controlled gas supplier (Shinyei SRG-1R-1, Japan). PXRD patterns at any given set RH were taken as follows. First, the specimen was kept under a N_2 flow (RH ca. 2%) for 1 or 24 h, depending on the sample's inherent behavior. Then, the relative humidity was raised in increments of 10% waiting 15 min in each step. Finally, the patterns were recorded at the desired RH value. The basal spacing $d003$, which is the c value of the subcell (one-third of the unit cell) containing one interlayer space, was estimated from both the 003 and the 006 reflections.

Results and Discussion

1. Characterization of Nitrate-Intercalated LDHs. Well crystallized LDH particles were chosen to perform this structural study to minimize the likely noise that the textural characteristics of polycrystalline solids may introduce. Two different well crystallized carbonate Mg(II)−Al(III) LDHs were converted into nitrate forms;[24,25] commercial carbonate HT bearing an Al(III) to Mg(II) ratio of 3, and a synthetic one having a ratio of 2 were employed as starting materials. It is worth mentioning that attempts to achieve other stoichiometries were unsuccessful, regardless of the initial or nominal Al(III) to Mg(II) ratio.[26,27] To explore a wider range of Me(II) to Al(III) ratios, an additional family of crystalline Al(III)−Ni(II) LDHs was prepared by hydrothermal homogeneous precipitation.[20−22] PXRD revealed for all TK samples a LDH structure with 3R symmetry that is characteristic of Takovite. Well dispersed hexagonal platelets were obtained (Figure S2 of the Supporting Information); FTIR and elemental analysis confirmed the expected pure carbonate−LDH form, in good agreement with previous reports.[28−31] TK samples were also exchanged quantitavely to the nitrate form. Table 1 presents the chemical composition of all studied LDHs samples; the numbers accompanying the acronyms indicate the divalent to trivalent cation mole ratio of each sample. For a given LDH, the layer charge density (e/Å^2) can be calculated as $x/a^2 sin\ 60°$, wereas a accounts for the inherent cation to cation distance within the xy plane and x the Al(III) mole fraction.[32]

2. Hydration-Mediated Expansion of HT. Sample HT2 was dehydrated in situ, in the PXRD chamber (Experimental Section) by exposing it to a 2% RH N_2 flow for 1 h. Figure 1 depicts the evolution of the PXRD patterns during the hydration of sample HT2. Initially, this phase exhibits an interlayer distance of 8.85(1) Å, in agreement with previous reports. This distance is ascribed to NO_3^- anions adopting a tilted, T in what follows, configuration of their C_3 axis respect to the xy plane.[9,11,12] As RH increases, the peaks corresponding to 003 and 006 interlamellar reflections shift toward lower angles in a continuous fashion, without exhibiting peak broadening or asymmetry. After reaching the highest relative humidity, a moderate interlamellar expansion of 0.1 ± 0.01 Å is observed (Figure 2). The slight expansion observed during this process started with galleries holding already tilted nitrate anions, and will be represented as $T \rightarrow T(h)$. In contrast with HT2, sample HT3, after 1 h dehydration, exhibits 003−006 interlamellar peaks corresponding to a distance of 7.8 ± 0.02 Å, close to that observed for the parent carbonate form of HT (Figure 3).[33] In this case, nitrate anions remain flat within the galleries, with their C_3 axis perpendicular to the LDH's xy plane of the octahedral sheets. However, once RH reaches 8%, both peaks shift toward lower angles, with a noticeable loss of symmetry. Phase segregation is evidenced by the incipient peak splitting observed at RH 12%. At RH = 22%, an expanded phase is evident in the PXRD pattern, indicating that the inclusion of water molecules within the interlamellar space exerts an abrupt expansion (0.6 Å) of the interlayer distance. Spectroscopic data recorded for a HT of similar composition revealed the existence of nitrate in the T form.[12]

A detailed inspection of the 003 peaks revealed very asymmetric shapes; attempts to fit those peaks as the sole contribution of an expanded and a nonexpanded phase, were unsuccesful, thus excluding a simple F to T phase expansion.

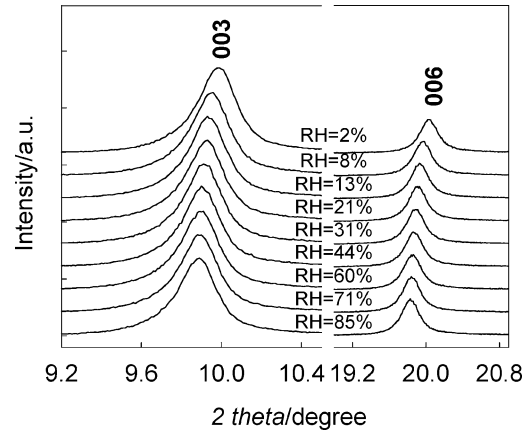

Figure 1. Structural evolution of sample HT2 exposed to increasing RH.

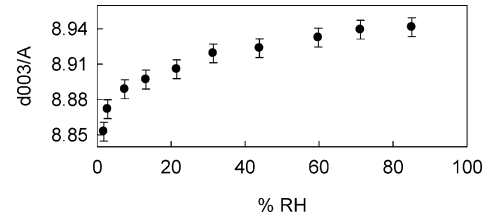

Figure 2. Evolution of interlamellar distance as a function of increasing RH, for sample HT2 in the tilted (T) form.

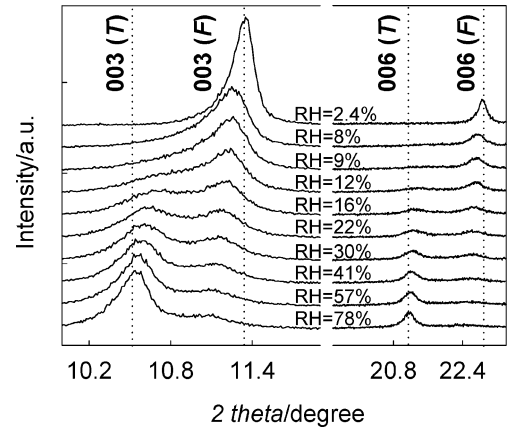

Figure 3. Structural evolution of sample HT3 exposed to increasing RH. Dotted lines depict the positions of the *003* and *006* reflections of the nonhydrated (F) form and the hydrated (T) one.

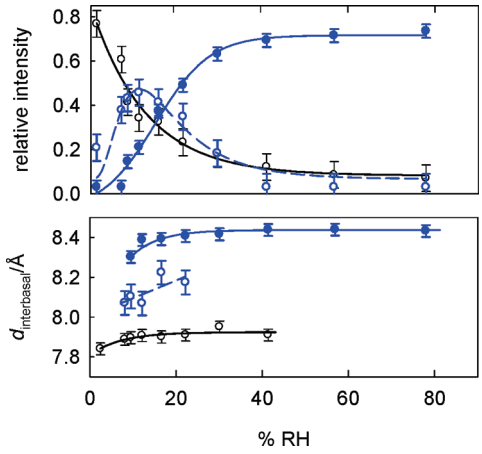

Figure 4. Relative abundance (upper view) and interlamellar distance (lower view) of the *F* (empty black circles), *SS* (empty blue circles), and *T* (filled blue circles) forms of sample HT3 as a function of increasing RH.

Introduction of a third phase characterized with an intermediate interlamellar distance was necessary to describe the observed peak profile (Figure S3 of the Supporting Information); moreover, this third phase exhibits the average distance of the expanded and nonexpanded ones. Figure 4 depicts the modification of the interlamellar distance of the three identified phases; their relative abundance (inferred from their intensity or peak's area) is also plotted.

Recent reports described the occurrence of partially hydrated phases characterized by a second staging array of *T* and *F* galleries.[10] In such structures, the more intense interlamellar reflection (indexed as 006) corresponds to the half *c* distance of unit cell of the second staging (*SS*) phase.[24] This behavior is not restricted to flat anions, such as nitrate, since it also was observed for HT intercalated with I^-, ClO_4^-, acetate, or propionate.[10,24] Then, the observed expansion can be described in terms of a hydration driven $F \leftrightarrow SS \leftrightarrow T$ sequence.

3. Dehydration-Mediated Contraction on HT. PXRD patterns in Figure 1 indicate that sample HT2, in contrast to HT3, failed to adopt the *F* configuration. Because dehydration of certain LDHs depicts hysteresis,[10] sample HT2 was submitted to a longer dehydration step, to assess any possible kinetic effects. Figure 5 depicts the structural evolution of sample HT2, driven by abrupt RH decrease from 40% to ca. 2%. After the first hour, sample HT2 suffers only a slight contraction, reverting from the initial *T*(*h*) state to the *T* one, in accordance with the hydration experience. This period is in fact an induction time for ensuing massive transformation and after 4 h of drying the *SS* phase becomes predominant. Then, at a lower pace, the latter phase evolves into the totally dehydrated *F* form.

In contrast with sample HT3, more structural details can be envisaged in this case, due to the inherent differences between the interlamellar distances of the hydration end members (Figure 6). From the variation of the observed interlamellar distances of *T* and *F* phases, a structural dehydration sequence $T(h) \rightarrow T \rightarrow SS \rightarrow F(h) \rightarrow F$ can be distinguished. Moreover, a $SS(h) \rightarrow SS$ step, which is the expectable evolution from a $T + F(h)$ to a $T + F$ second staging array, can also be observed. It is worth noting the inherent deceleratory dehydration regime, because the overall step $T(h) \rightarrow T$ takes less than 5 min, whereas the $T \rightarrow SS$ step takes 2 h and the final $SS \rightarrow F$ step almost a day, respectively.

Interestingly, the final dehydrated *F* form once resubmitted to ambient RH, it rehydrates completely to the *T*(*h*) initial state

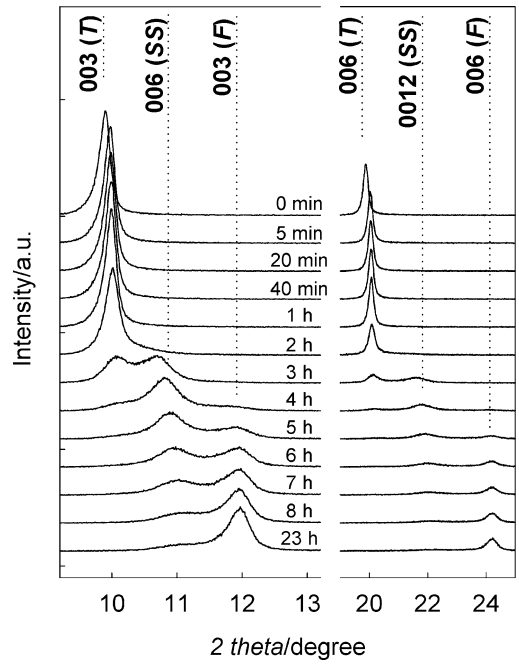

Figure 5. Structural evolution of sample HT2 during dehydration at 2% RH. Dotted lines depict the position of the *003* and *006* reflections of the starting nonhydrated *F* form and the final hydrated *T*(*h*) forms, and of the interlamellar *006* and *0012* reflections of the *SS* intermediate phase.

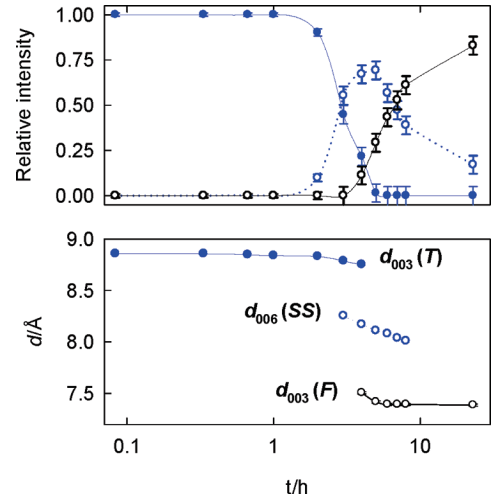

Figure 6. Structural modification of sample HT2 during dehydration at 2% RH. Evolution of the relative abundance (upper view) and the interlamellar distance (lower view) of the *T* (filled blue circles), *SS* (empty blue circles), and the *F* (empty black circles) one.

in a matter of minutes (Figure S6 of the Supporting Information), say 2 orders of magnitude faster than dehydration. This apparent kinetic irreversibility of can be interpreted in terms of the structural changes driven by the deintercalation of water molecules from a single crystal LDH. Previous reports dealing with intercalation reactions in single crystalline layered compounds revealed a stepwise process, with each steps governed by pure phases, characterized by a defined structure and intercalation degree. Ganal et al. demonstrated that first intercalation phase nucleate in the borders, where the gradient is maximum, and then grow toward the center of the crystal, following a cylindrical symmetry regime (Scheme 3 of the Supporting Information).[34] Extrapolating that behavior to the present case, the initial release of intercalated water molecules prompts dehydration of the edges of the galleries of the *T* form,

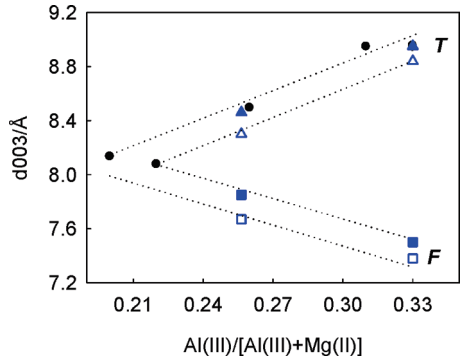

Figure 7. Interlamellar distance of HT samples in the *F* configuration of a nonhydrated state (empty blue squares), a hydrated *F*(*h*) state (filled blue squares), a *T* configuration (empty blue triangles), and the *T*(*h*) one (filled blue triangles), as a function of Al(III) substitution. Literature data (black circles, ref 9) are also presented.

until the *SS* phase nucleates. On growing toward the center of the crystal, this phase occupies practically the whole crystal volume, and consequently defines the observed PXRD pattern. Structural data suggest that water migration through *F* galleries should be sluggish as compared to water migration through the *T* ones, due to the minimum free space left between nitrate anions. Thus, once the galleries at the borders are predominantly dehydrated in the *F* form, water molecules must remain trapped in this sealed inner crystal, thus the slower advance of the *F* front makes the final *SS* → *F* step even more dawdling than the previous ones. In addition, the mean distance that a water molecule should travel through an *F* gallery to leave the crystal increases during this last step, resulting in a deceleratory dehydration rate. It is worth mentioning that the *SS* and *F* phases present broader reflections, suggesting smaller size domains (in the *z* direction) than the parent *T* form. This suggest that the aforementioned process takes place independently on different borders of each crystal, in line with the more elaborated models proposed for molecular intercalation of layered phases.[35]

Interestingly, the aforementioned dehydration stepwise process was not observed for sample HT3, which dehydrates completely to the *F* configuration in less than 1 h. Sample HT3 dehydrated for 24 h rehydrates in a similar way as the one dehydrated for 1 h. A lower charge density in LDH implies less nitrate anions in the gallery, and more free space to allow the water migration, allowing a faster dehydration process.

4. Phase Domains of HT Phases. Besides the discussed kinetic aspects, the structural implications of water uptake, and the occurrence of the so-called abrupt phase transition deserves to be revisited.[9] Figure 7 compiles the values of the *c* parameter of nitrate HT, including the extreme phases (the *F* and *T*(*h*) one) observed for HT2 and HT3. Both HT samples shift discontinuously from the *F* configuration to the *T* one through the *SS* intermediary phase. However, for both configurations, incoming water expands the gallery only in a slight manner, ca. 0.1 Å,[36,37] being solely the relative abundance of each type of interlamellar array the main structural effect of water uptake. Previous structural and spectroscopic observations of less defined structures are the natural result of partially hydrated phases, in which *F* and *T* arrays coexist in the otherwise pure LDH.

5. Hydration-Mediated Expansion and Phase Domains of TK Phases. To explore the behavior of nitrate LDHs having a wider charge density range, the behavior of a whole TK family (Table 1) was also studied by PXRD as function of RH, after a 1 h dehydration step, exclusively. Samples TK2.5 and TK3, bearing intermediate charge densities behaved similarly to HT3,

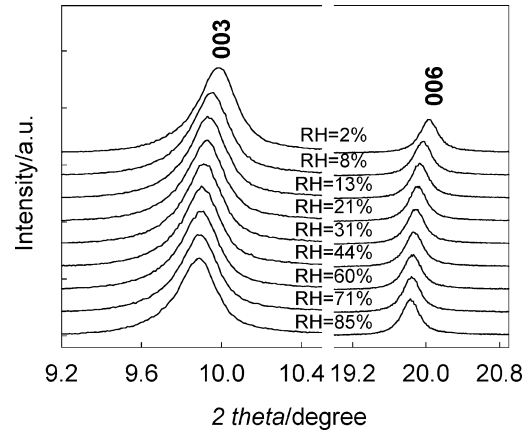

Figure 8. Structural evolution of sample TK4 exposed to increasing RH.

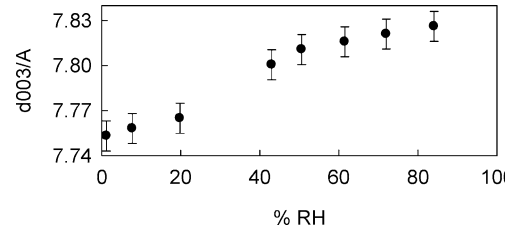

Figure 9. Evolution of interlamellar distance of sample TK4 as a function of RH.

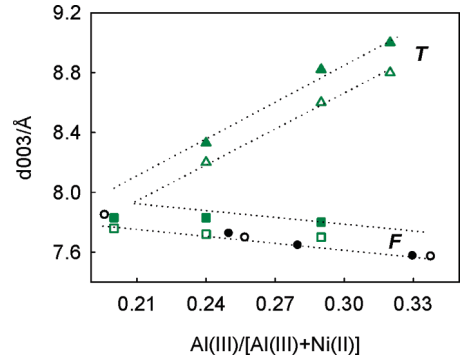

Figure 10. Interlamellar distance of Takovites as a function of Al(III) substitution, for carbonate (data taken from ref 30 full circles, and ref 31 empty circles) and nitrate Ni(II)−Al(III) LDHs in a nonhydrated *F* configuration (empty green squares), in a *F*(*h*) hydrated configuration (filled green squares), a poorly hydrated *T* configuration (empty green triangles), and highly hydrated *T*(*h*) one (filled green triangles).

exhibiting an analogous *F* → *T* transition (data not shown) with the occurrence of a *SS* intermediary phase.

Sample TK2 followed a *T* → *T*(*h*) continuous shift, in good agreement with sample HT2. However, sample TK4, bearing the lowest charge density, exhibited an almost invariant behavior, with a slight and continuous expansion of ca. 0.1 Å (Figures 8 and 9). The *F* phase is stable along the whole range of RH, and only the *F* → *F*(*h*) hydration step was observed, without any change in the shape or FWHM of the diffraction peaks, as it was observed for the *T* → *T*(*h*) transition of sample HT2 (Figure 1).

Except for sample TK4, the *T*(*h*) and the eventual *F* forms observed of all the other TK samples followed the expansion trend observed for HTs ones. Figure 10 presents the structural trend depicted by the TK family; the values reported for carbonate forms of TK are also presented.[30] In general, TK samples matches with the behavior of the HT ones, except for

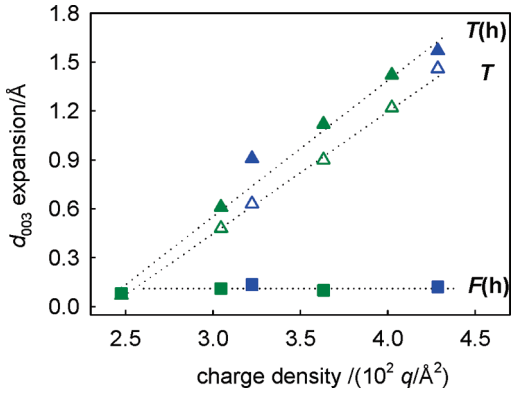

Figure 11. Net interlamellar expansion from the totally dehydrated form as a function of layer charge density. Filled squares, open triangles, and filled triangles represent the $F \rightarrow F(h)$, $F \rightarrow T$, and $F \rightarrow T(h)$ expansions, respectively; green symbols corresponds to the TK family, blue symbols to the HT one.

a slight difference of d_{003} (0.2 Å). This fact obeys to the difference in the layer thickness when Mg(II) is replaced by Ni(II); the 001 distance of the parent $Mg(OH)_2$ and β-$Ni(OH)_2$ phases are 4.7683 Å and 4.6074 Å, respectively.[38,39] For intermediate layer charge densities, nitrate forms of LDHs are able to jump with no major kinetic hindrance from T to F configurations, when RH increases, favoring the hydration of the gallery and diminishing lateral repulsion, in detriment of the anion-layer attractive interaction. Higher charge density TKs require longer exposures to drying conditions to adopt the flat configuration, as HT samples do.[10] For both TK and HT families, F phase contracts when charge density increases, indicating that in the absence of water the attractive force between the layers and the anions prevails over the lateral nitrate to nitrate repulsive one. The correspondent T forms show an opposite trend, governed by the optimization of hydration interactions over the electrostatic attraction. The absence of an abrupt transition for sample TK4 can be envisaged as the convergence of the T and the F interlayer distances to a common magnitude.

6. General Hydration Behavior of Nitrate LDHs. In the search of a general description that accounts for the dissimilar behaviors observed for rather similar samples, it would be worth finding which is the structural parameter that governs water driven expansion. Focusing on the charge density that defines the average nitrate to nitrate distance, the extreme cases, such as TK4 and HT2, denote the tendency of nitrate anions to remain in the F and the T configurations, respectively. Intermediate samples can be easily transform into one another by means of hydration-dehydration. Figure 11 summarizes the behavior of all the studied samples, presenting the net interlamellar expansion (taking the initial dehydrated forms F as reference) as a function of the charge density of the xy plane. For all LDHs, only a 0.1 Å expansion is observed, after the first $F \rightarrow F(h)$ hydration step, irrespective of the charge density. All the samples, except TK4 and TK2, exhibited the sequence $F \rightarrow F(h) \rightarrow SS \rightarrow T \rightarrow T(h)$. An analogous slight and continuous expansion of ca. 0.1 Å is also observed during the final $T \rightarrow T(h)$ hydration step. Along the whole range of charge density that most LDH can bear, the galleries can evolve from a non expanded hydrated condition to an expanded one in which nitrate stands with its C_3 axis depicting increasing angles respect to the layer's xy plane, as higher becomes the xy plane charge density. It is in the magnitude of the net difference between the $F(h)$ and T phases were the layer's charge density (or average nitrate to nitrate distance) exerts its dramatic influence.

Conclusions

Instead of a single abrupt expansion proper of certain of HT with certain Mg(II) to Al(III) ratio, many nitrate-intercalated LDHs develop a abrupt expansion, once submitted to increasing water activity. For lower charge densities, the electrostatic attraction between the anions and the sheets prevails over other interactions and the anions remain flat, irrespective of water activity. As the charge density increases, these phases are able to modify the orientation of the anions to optimize the balance between the columbic forces (attraction by the positive brucitic layers and repulsion between them) and the molecular interactions involving interlayer water (solvation and hydrogen bonding with the anions and the structural OH groups). The transition to the expanded form is discontinuous, and involves SS intermediary phases; the maximum gallery expansion achieved is proportional to the layer charge density. This process is easily reverted after a short-term drying process for LDH bearing intermediate x values. For highly charged layers, the average distance between nitrate anions decreases sufficiently to hinder the release of water forced by dehydration, resulting in a well-defined $T \rightarrow T(h) \rightarrow SS \rightarrow F \rightarrow F(h)$ sequence. The rigorous structural inspection of LDH phases requires adequate control of RH. The occurrence of a structural transition can be properly observed and described only if well-crystallized solids, which minimize the overlapping of diffraction signals of the involved hydration phases, are inspected.

Acknowledgment. This work was supported by Grant-in-Aid for Scientific Research (c) (20550142) of JSPS (Japan Society for the Promotion of Science), the University of Buenos Aires (UBACyT X-003 and X-081), Agencia Nacional de Promoción Científica y Tecnológica (ANPCyT PICT 06-33973), and by The National Research Council of Argentina (CONICET PIP 112-200801-02533269). We are deeply indebted with Dr. A. E. Regazzoni for his helpful comments and corrections. M.J. is a member of CONICET and Gabbo's.

Supporting Information Available: PXRD patterns of the starting carbonate TK samples as well as a representative SEM image of the TK crystals. Detailed PXRD patterns of partially hydrated HT samples. Schemes depicting the structural changes driven by hydration. This material is available free of charge via the Internet at http://pubs.acs.org.

References and Notes

(1) Rives, V. *Layered Double Hydroxides: Present and Future*; 2001.
(2) Parise, J. B.; Leinenweber, K.; Weidner, D. J.; Kemin, T.; Von Dreele, R. B. *Am. Mineral.* **1994**, *79*, 193.
(3) Evans, D. G.; Slade, R. C. T. Structural aspects of layered double hydroxides. In. *Struct. Bonding (Berlin)* **2005**, *119*, 1.
(4) Sideris, P. J.; Nielsen, U. G.; Gan, Z. H.; Grey, C. P. *Science* **2008**, *321*, 113.
(5) Ennadi, A.; Legrouri, A.; De Roy, A.; Besse, J. P. *J. Solid State Chem.* **2000**, *152*, 568.
(6) Prasanna, S. V.; Radha, A. V.; Kamath, P. V.; Kannan, S. *Clays Clay Miner.* **2009**, *57*, 82.
(7) Miyata, S. *Clays and Clay Minerals* **1983**, *31*, 305.
(8) Israëli, Y.; Taviot-Gueho, T.; Beese, J. P.; Morel, J. P.; Morel-Desrosiers, N. *J. Chem. Soc., Dalton Trans.* **2000**, 791.
(9) Xu, Z. P.; Zeng, H. C. *J. Phys. Chem. B* **2001**, *105*, 1743.
(10) Iyi, N.; Fujii, K.; Okamoto, K.; Sasaki, T. *Appl. Clay Sci.* **2007**, *35*, 218.
(11) Li, H.; Ma, J.; Evans, D. G.; Zhou, T.; Li, F.; Duan, X. *Chem. Mater.* **2006**, *18*, 4405.
(12) Wang, S. L.; Wang, P. C. *Colloids Surf., A* **2007**, *292*, 131.
(13) Marcelin, G.; Stockhausen, N. J.; Post, J. F. M.; Schutz, A. *J. Phys. Chem.* **1989**, *93*, 4646.
(14) Hou, X. Q.; Kirkpatrick, R. J.; Yu, P.; Moore, D.; Kim, Y. *Am. Mineral.* **2000**, *85*, 173.

(15) Toraishi, T.; Nagasaki, S.; Tanaka, S. *Appl. Clay Sci.* 2002, *22*, PII S0169.
(16) Chao, Y. F.; Chen, P. C.; Wang, S. L. *Appl. Clay Sci.* **2008**, *40*, 193.
(17) del Arco, M.; Gutierrez, S.; Martin, C.; Rives, V.; Rocha, J. *J. Solid State Chem.* **2000**, *151*, 272.
(18) Jobbagy, M.; Regazzoni, A. E. *J. Phys. Chem. B* **2005**, *109*, 389.
(19) Khan, A. I.; O'Hare, D. *J. Mater. Chem.* **2002**, *12*, 3191.
(20) Jobbagy, M.; Blesa, M. A.; Regazzoni, A. E. *J. Colloid Interface Sci.* **2007**, *309*, 72.
(21) Liu, Z. P.; Ma, R. Z.; Ebina, Y.; Iyi, N.; Takada, K.; Sasaki, T. *Langmuir* **2007**, *23*, 861.
(22) Okamoto, K.; Iyi, N.; Sasaki, T. *Appl. Clay Sci.* **2007**, *37*, 23.
(23) Soler-Illia, G.; Jobbagy, M.; Candal, R. J.; Regazzoni, A. E.; Blesa, M. A. *J. Dispersion Sci. Technol.* **1998**, *19*, 207.
(24) Iyi, N.; Ebina, Y.; Sasaki, T. *Langmuir* **2008**, *24*, 5591.
(25) Iyi, N.; Sasaki, T. *J. Colloid Interface Sci.* **2008**, *322*, 237.
(26) Costantino, U.; Marmottini, F.; Nocchetti, M.; Vivani, R. *Eur. J. Inorg. Chem.* **1998**, 1439.
(27) Ogawa, M.; Kaiho, H. *Langmuir* **2002**, *18*, 4240.
(28) Solin, S. A.; Hines, D.; Yun, S. K.; Pinnavaia, T. J.; Thorpe, M. F. *J. Non-Cryst. Solids* **1995**, *182*, 212.
(29) Bish, D. L.; Brindley, G. W. *Am. Mineral.* **1977**, *62*, 458.
(30) Brindley, G. W.; Kikkawa, S. *Am. Mineral.* **1979**, *64*, 836.
(31) Kovanda, F.; Rojka, T.; Bezdicka, P.; Jiratova, K.; Obalova, L.; Pacultova, K.; Bastl, Z.; Grygar, T. *J. Solid State Chem.* **2009**, *182*, 27.
(32) Li, L.; Ma, R. Z.; Ebina, Y.; Fukuda, K.; Takada, K.; Sasaki, T. *J. Am. Chem. Soc.* **2007**, *129*, 8000.
(33) Miyata, S. *Clays Clay Miner.* **1980**, *28*, 50.
(34) Ganal, P.; Butz, T.; Lerf, A. *Synth. Met.* **1989**, *34*, 641.
(35) Evans, J. S. O.; Price, S. J.; Wong, H. V.; O'Hare, D. *J. Am. Chem. Soc.* **1998**, *120*, 10837.
(36) Wang, J.; Kalinichev, A. G.; Kirkpatrick, R. J.; Hou, X. *Chem. Mater.* **2001**, *13*, 145.
(37) Perez-Ramirez, J.; Abello, S.; van der Pers, N. M. *Chem.—Eur. J.* **2007**, *13*, 870.
(38) JCPDSN°7−0239.
(39) JCPDSN°14−0117.

JP1078778